First steps to develop a triboelectric wind turbine for Mars exploration

[1]Borja Pozo*, Iban Quintana*, Ewelina Ryszawa**, Iñigo Muñoz*, Lionel Galliard**, Erlatnz Fernandez de Gorostiza*

Abstract

The aim of the work has been to develop the trade-off for the first wind turbine which will be an efficient and robust TEG demonstrator that can efficiently operate under Mars environmental conditions, consolidating the technical requirements considering the needs of the past, present, and future space missions. This work has investigated Mars fluidics operation behavior through a turbine, triboelectric materials and has performed a trade-off, with a particular focus on energetic efficiency, robustness, simplicity, scalability, easy mechanical integration, reduction of mass and weight of current turbines, minimization of cost and compatibility to present and future space developments.

Introduction

A consistent and reliable power supply is critical for future Mars missions. The idea is to use Mars winds to produce electrical energy and use it as an auxiliary energy source to solar cells during the Martian storms and continue low electric supply during the storms. However, the usual Electromagnetic Generators (EG) are unsuitable for planetary exploration due to their heavyweight, leading to the high launch costs. The alternative to EG can be the Triboelectric Generator (TEG), which produces more power than an EG when weight and volume are considered as key parameters [1][2]. This paper describes the operation principles, trade-off developments, and results of a first approach to implement the first wind turbine tests based on the TEG generator for Mars.

Even though on Mars there are wind seasons with high-speed winds, the atmosphere density is very low, so, it is not obvious that a wind turbine would move under those conditions. According to the power production equation, the extraction potential for wind power is a function of velocity cubed and only proportional to density. This means that the effect of the low density of the Mars atmosphere has smaller importance than the velocity regarding the power that can be extracted from the winds. In addition, two works of NASA and Houston University [3][4], made theoretical analyses about the possibility to generate energy from the wind with a different type of big size Vertical-Axis Wind Turbine (VWAT). The level of energy estimate was 19 kW in a 29 m/s wind considering a mass of 429 kg. The conclusions were that such system can work and generate enough energy; however, the generator design must be improved.

Besides the theoretical results that are presented in the mentioned two papers, in another work [5] it was demonstrated that wind power can be used on Mars to produce energy. In this work several tests in a wind tunnel were performed, in the Martian atmospheric environment to duplicate the atmospheric density from Mars. The turbine used in those tests had a quite simple design and the objective was not to maximize the power generation but to verify that a wind turbine can rotate under martian conditions and generate energy.

The important point to consider is the effect of Mars atmospheric conditions on the triboelectric principle. As it is described and analyzed in [6], if the TEG generator is packaged hermetically in CO_2 (and the pressure inside the package is maintained at 760 Torr), the output performance increases by 157% compared to Earth conditions. This dependence on atmospheric conditions can be explained by a charge relaxation model [7]. In this work, this effect has been tested and validated.

* Tekniker, Iñaki Goenaga 5, Eibar, 20600, Gipuzkoa, Spain; borja.pozo@tekniker.es
** ESA-ESTEC, European Space Agency - European Space Research and Technology Centre, Keplerlaan 1, 2201 AZ Noordwijk, The Netherlands; ewelina.ryszawa@esa.int

Proceedings of the 46th Aerospace Mechanisms Symposium, NASA Johnson Space Center, May 11-13, 2021

Mars atmospheric conditions and winds

The main atmosphere parameters that change on Mars regarding the Earth are density and velocity. The average atmosphere density on the Earth is 1.217 kg/m3 and on Mars 0.020 kg/m3, both at surface level. The wind speeds measured on Mars give a range between 5 and 30 m/s. The work presented in this paper has been developed using real data measured by NASA's Insight mission at the Elysium Planitia to find out how the turbine works in real Martian conditions. Fig.1 shows the measurements from the TWINS instrument used to measure the Mars weather since 2019, which has been used in this work as reference (from Mars InSight Weather Report). Pressure changes due to the seasons and the average, minimum, and maximum wind velocities are shown:

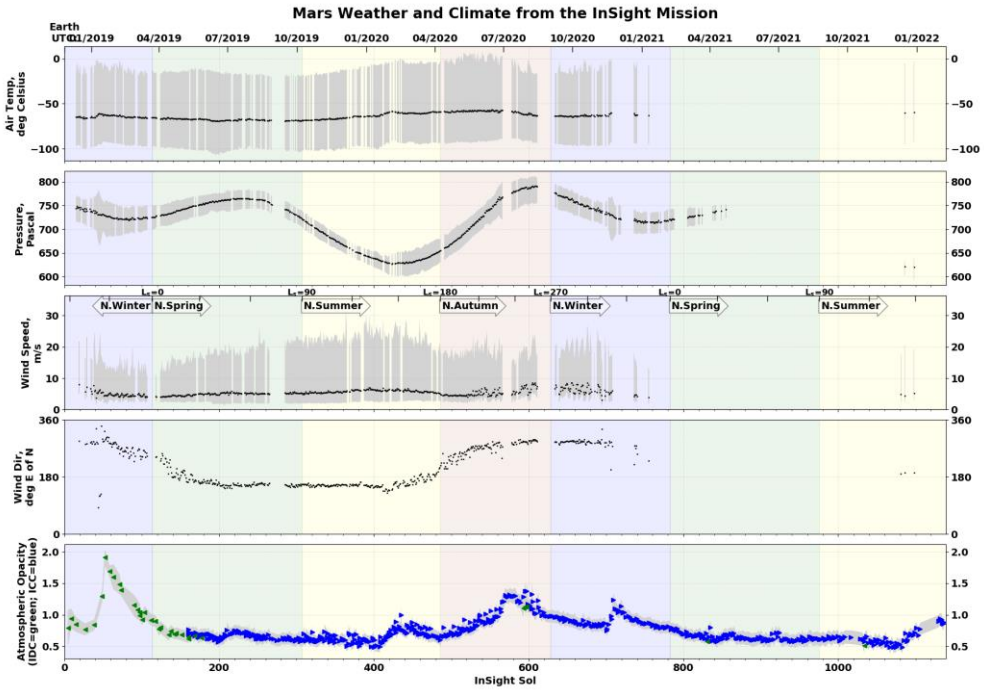

Figure 1. Atmospheric parameters mesuared by Insight in Mars (figure from NASA).

Diurnal and subdiurnal variability on Mars, with its uniquely low average surface pressure, highlights an end-member case of sunlight control of the diurnal cycle, particularly as compared to Earth. This causes on Mars (relative to Earth):

1- Atmospheric thermal tides an order of magnitude stronger, especially in low latitudes.
2- More sustained daytime upslope and night-time downslope flows, especially over steep slopes.
3- A much sharper contrast between the strong daytime, buoyancy driven convective turbulence and the moderate night-time, shear driven mechanical turbulence.

Wind turbine

Selection of wind turbine type

For the design of the wind turbine, the first aspect that has been studied is the type of turbine that best meets the requirements. The first step for defining a type of wind turbine is to analyze the two principal designs in terms of the orientation of the rotor axis. Wind turbines can be classified as Horizontal Axis Wind Turbines (HAWT) and Vertical Axis Wind Turbines (VAWT). Although VAWTs have fallen significantly behind HAWTs in recent years in terms of technical development and in the number of units manufactured, they have some advantages that made them suitable for some applications. The main difference between both types of turbines is that VAWTs are crossflow devices and accept wind from any direction while in HAWTs the rotor must be kept perpendicular to the flow of the wind, which means that it must be oriented to capture the maximum energy from the wind. Moreover, in VAWTs the components may be connected

directly to the rotor shaft and located at the ground level. This eliminates the need for a tower to support the weight of equipment such as the gearbox and other main turbine components. Due to the extreme weather, the Martian dust and the weight limitations, the absence of the orientation mechanism and the ease of operation, maintenance, lifetime, and installation are the key aspects when choosing the type of turbine for this application. Therefore, a vertical axis wind turbine (VAWT) best meets the requirements.

Design of the wind turbine

The main dimensions of the rotor, the number of blades, the airfoil and its chord length, the rotor strength, and the pitch angle have been defined. For this purpose, literature references are sought, and Q-blade software was used to simulate the rotor by varying its design parameters. This software is based on the model of moments, and although it does not consider the stall, it allows to obtain very fast results being a very useful tool for the design process. The main dimensions of the rotor are defined, which are height (H) and diameter (D). From these two parameters, both the swept area and the aspect ratio of the rotor are defined and shown in Eq.1 and Eq. 2.

$$Swept\ Area\ (m^2) = H\ x\ D \qquad \textit{Equation 1}$$

$$Aspect\ Ratio\ (-) = \frac{H}{R} \qquad \textit{Equation 2}$$

Considering that the whole system will be tested inside the wind tunnel of the University of Ahrus, there are some dimensional limitations). The wind tunnel is a rectangular cavity of one meter high by two meters wide. It is estimated that the TEG itself will have between 10 and 20 centimeters high, and, in addition, it will be necessary to leave some height in relation to the tunnel ceiling. These two limitations mean that only 0.7 meters of height is available for the rotor. Considering that the larger the swept area the higher the power output and that there is less margin in terms of height, the rotor height has been set to its maximum value, that is H=0.7 m. Then, the diameter has been adjusted, considering the aspect ratio. Reviewing [8][9], it is concluded that if blade tip losses are considered, high aspect ratio values should be used. If the structural aspect is also considered, aspect ratio values between 2.5 and 3 are recommended. By simulating three different diameters that meet this requirement, the diameter is set at D=0.5 m. For the blades definition, the references [10]-[13] indicate that increasing the number of blades decreases the efficiency of the rotor due to interference between the blades. However, the use of more blades balances the turbine and makes the torque generated more constant [14]. Discarding the use of 1 blade (many balancing problems) and 4 blades (very low efficiency), two rotors of 2 and 3 blades respectively were simulated in Q-Blade. The results show higher power coefficients over a wider operating range when three blades are used. As for the aerodynamic profile of the blades, there are several options, many of which have been developed for use in VAWTs [15] [16]. For simplicity, it has been decided to use a symmetrical airfoil. After running some simulations, NACA0018 will be used because of its good performance and because it is structurally strong enough. Once the airfoil is known, its dimensions must be defined. The chord length is defined as the distance between the leading edge and the tail of the airfoil. This parameter directly affects the solidity of the rotor which is defined in Eq. 3:

$$\sigma = \frac{Number\ of\ blades\ x\ Chord\ length}{Rotor\ radius} \qquad \textit{Equation 3}$$

The various studies recommend solidities of between 0.2 and 0.5, and it is known that the rotor has a self-starting capability only at solidities greater than 0.4 [17]. Due to the higher power coefficient and a wide operating range and considering other factors such as self-starting capability and cost, the solidity is set at 0.4. This implies that the blades will have a chord length of 0.035m.The last parameter to configure is the pitch angle. The pitch angle may be positive, if the leading edge of the airfoil points towards the center of the rotor, or negative if it points away from the rotor. From the literature, it is concluded that positive pitch angles decrease performance while negative pitch angles increase performance if they are between 0º and 2º [18][19].After simulating different pitch angles in QBlade the conclusion is that the performance is very similar. In order not to complicate the design, the pitch angle will be left at 0º. Tab. 1 summarizes the selected values:

Table 1. Main rotor selected parameters.

Parameter	Value	Parameter	Value
Height (m)	0.7	Chrod length (m)	0.035
Diamater (m)	0.5	Solidity	0.4
Number of blades	3	Pitch angle (º)	0
Airfoil	NACA0018		

FEM Simulations

The analysis of the wind turbine using the finite element method (FEM) can be divided into two types of analysis, thermo-fluidic analysis, and mechanical analysis. The thermo-fluidic analysis focuses on obtaining temperature and pressure contours, as well as forces that can be caused by fluids in different solids. The results can be used as input loads to the mechanical analysis where the objective is to study the mechanical behavior of the system by analyzing among other things stresses and deformations. Both analyses have been carried out through several simulations in ANSYS software.

As it is known, wind at a certain speed will impact the blades of the wind turbine, causing a rotational movement around its axis, which will accelerate until it reaches a constant rotational speed. The aim of this analysis is to study the interaction between the wind and the rotor, which will allow us to obtain the performance and the self-starting capacity of the wind turbine itself, as well as the forces exerted on it in different positions and moments. These simulations are all carried out in 2D, as is shown in Fig 2. The geometry for CFD simulations is divided into two parts, a rotating part (rotor domain) and a fixed part (outer domain). The dimensions of the outer domain are those of the wind tunnel, so the width is 2 m while the length is 7 m. The rotor is located 3 m from the tunnel entrance where the velocity inlet boundary condition applies and 4 m from the exit where the pressure outlet boundary condition applies. As for the sidewalls, when the rotor is simulated inside the wind tunnel, they will have a wall boundary condition while when simulated in the Martian environment they will have a symmetry boundary condition.

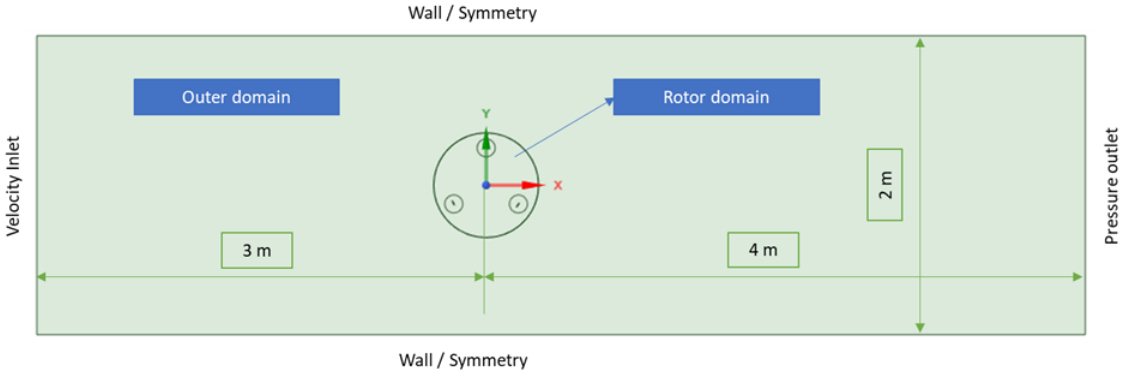

Figure 2.Geometry and boundary conditions for CFD simulations.

To ensure that wind turbulence is well captured in the areas close to the wind turbine blades it is necessary to mesh these areas more finely. For this purpose, a subdomain is defined around each of the three blades. In this case, the moving part of the mesh, that is the rotor, moves according to the wind, which in turn is affected by the rotor itself. For this reason, since the rotational velocity of the wind turbine is to be obtained as a function of wind velocity, the 6DOF model must be used. In this model, the inputs have been the mass and moment of inertia of the rotor. To calculate them, the blade material has been selected as carbon fiber. Finally, the CO2 has been set as a simulation fluid, however, its properties will vary depending on pressure and temperature, where the data has been obtained from the National Institute of Standards and Technology (NIST).

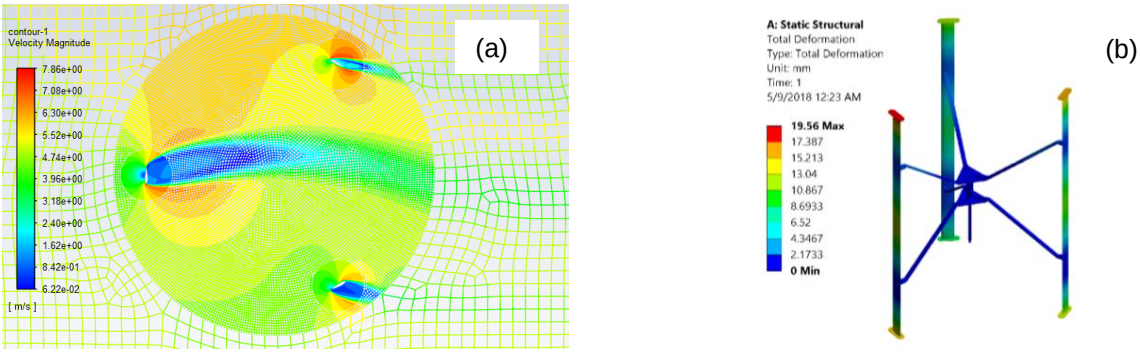

Figure 3. Contour of velocities at two different instants obtained using the 6DOF model. a) Contour of velocities at two different instants obtained using the 6DOF model. b) Structural analysis of the designed turbine.

The CFD simulations have been divided into several packages depending on the results and conclusions to be drawn: Self-starting, Testbench, Mars, and Structural. In the “self-starting” package, the objective has been to determine the minimum necessary conditions that are needed for the wind turbine to operate. The aim is to validate if the turbine is capable of self-starting and generating sufficient torque under the most unfavorable conditions. The objective of the “Testbench” package is to simulate the rotor under test bench conditions, while the “Mars” package is to simulate the rotor under real Martian conditions. Finally, the objective of the “Structural package” is to see if the wind turbine can structurally withstand the loads expected during its operation on Mars (currently, launch loads are not considered within the space of the current work). Therefore, the rotor is subjected to the most extreme conditions both on the testbench and on Mars to obtain the rotational speeds and the forces exerted by the wind. The following table shows the results obtained in all simulations in terms of rotational speed and self-starting time. In addition, the acceleration graph of the simulation package "Test-bench" is shown in Fig. 4.

Package	ID	Scenery	Angular velocity (r.p.m)	Self-start time (min)
Self-start	Self_01	Mars	12,4	13
	Self_02	Test-bench	10,8	12,2
Test-bench	TB_01	Test-bench	10,8	12,2
	TB_02	Test-bench	40,6	40
	TB_03	Test-bench	78,9	15,7
	TB_04	Test-bench	114,5	12,8
	TB_05	Test-bench	117,7	14,3
	TB_06	Test-bench	138,2	7,5
Mars	InS_01	Mars	264	5,83
	Ins_02	Mars	116	13,3
	Ins_03	Mars	168	5
	Ins_04	Mars	168	5
Structural	SF_01	Mars	384	2,3
	SF_02	Mars	433	2,2
	SF_03	Test-bench	114,5	12,8
	SF_04	Test-bench	138,2	7,5

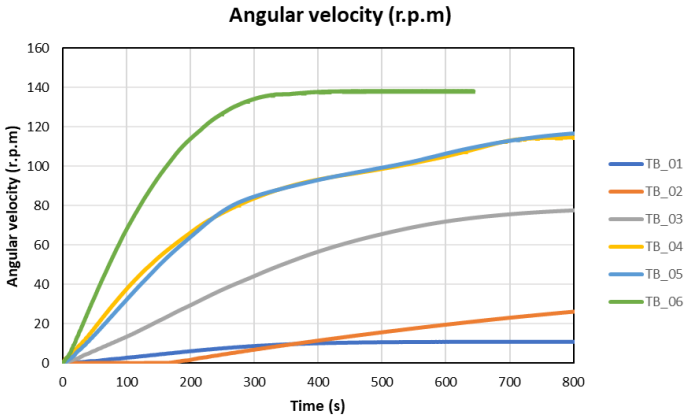

Figure 4. Rotational velocities and self-starting time for all the simulations carried out and acceleration graph for "Test-bench" package.

It is validated that the turbine accelerates until it reaches a constant speed, the time it takes to accelerate being the self-starting time.

Triboelectric generator

Triboelectric effect operational principles

The triboelectric generation consists of the electric charge transfer between two materials by friction. In the triboelectric configuration of this work, the rotor material will be prone to become positively charged, while the stator material will be prone to become negatively charged. Based on their triboelectric properties, their ability to lose or gain electrons, aluminum (Al) and polytetrafluoroethylene (PTFE) can be considered for the rotor and stator, respectively. The functionality of TEGs is based on triboelectrification (or contact electrification) and electrostatic induction phenomena. The TEG architecture involves two materials with different charge affinity during contact. The freestanding TEG has more advantages than a contact separation mode as it does not require attachment to the moving triboelectric layer with an electrode and a lead wire. In this work, a freestanding mode has been selected as generator architecture.

To further assess the effect of the geometry and dimensions of the triboelectric generator on the generation of the electrostatic potential, finite element simulations have been performed using FEMM (Finite Element Methods Magnetic) software. It must be remarked that only the electrostatic induction phenomenon has been simulated, assuming a given charge density generated by the friction between rotor and stator. Parametric variations of the following geometric parameters have been simulated as can be seen in Fig. 5:

- N: Number of poles (blades), affecting the cross-section of each pole
- t: stator conductor thickness
- g: gap between insulated stator conductor sections

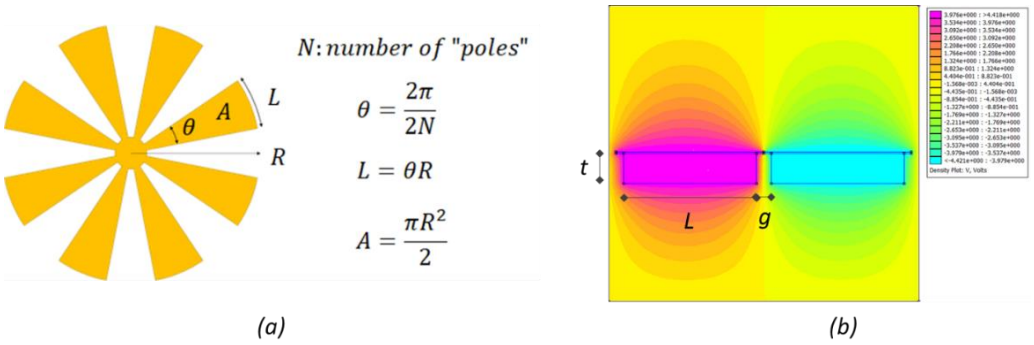

Figure 5. Paremeters for electrostatic simulations and simulation example.

In this scenario, a grating structure is manufactured in the rotator and stator, where the output power depends on the material selection, contact surface characteristics, grating number, and electrode gap.

The simulations gave the results shown in Fig. 6. Fig. 6a shows the simulation results obtained when varying the thickness of the conductors at the stators where the electrostatic potential is induced. Fig. 6b shows the simulation results with further varying of the gap from 5 to 30mm.

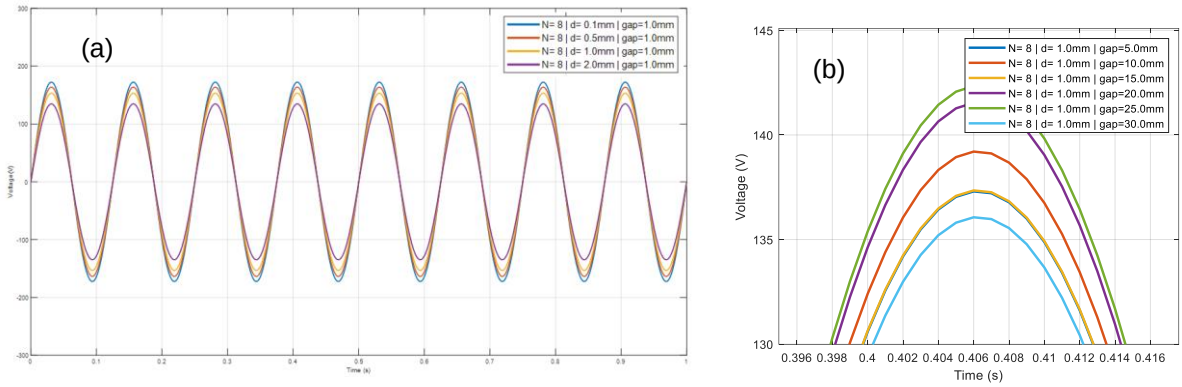

Figure 6. Results achieved with the electrostatic simulations. a) Output voltage vs. conductor width. b) Output voltage vs. gap length.

It has been observed that for a given charge density, the amplitude of the induced voltage is independent of the number of poles. At the same rotational speed, the frequency of the induced voltage increases with

the number of poles. It is assumed that a higher number of poles will result in a more homogeneous charge distribution by friction between the rotor and stator. On the other hand, if a homogeneous charge distribution is assumed for the electrostatic induction simulation, the effect of the number of poles cannot be appreciated. It can be observed that the induced voltage amplitude decreases with increasing conductor thickness. This might be caused by the electric charge concentration on the surface of the conductor (in a very thin layer of the order of nm) and is not affected by the considered conductor thicknesses. The electric field generated by the electric charge on the triboelectric surface decreases with distance and the smaller the thickness of the conductor, the greater the electric field inside the conductor and the greater the induced voltage. It can be observed how the amplitude of the induced voltage starts increasing as the gap between conductors increases, but at a certain point, the effect is reversed. On one hand, as the gap between conductors increases, the conductors lie within more intense electric field regions; but on the other hand, the area of the conductors will directly affect the distribution of electric charges inside the conductors. Thus, for the final configuration, the best equilibrium between the gap and conductor area will have to be searched.

Tribopair selection

The TEG concept could harvest both low and high wind speed which made it very attractive for energy harvesting on Mars, with a broadband external wind speed range. It has required to use of advanced triboelectric materials that have a combination of excellent tribological performance (low friction and wear), mechanical (impact resistance), triboelectric properties (triboelectrification and interfacial conductivity), and energy generation density under those extreme conditions, under a freestanding mode.

The pre-selection of these materials, which will be considered as rotor and stator components of the TEG, has been validated by performing pin-on-disc tribological tests under low-pressure conditions (P=6mbar) and CO_2 environment, as shown in Fig. 7a. The test conditions considered have been: Contact pressure of 11MPa, a stroke of 3mm, and a sliding velocity of 3mm/s. Test duration was fixed to 80000 s after preliminary trials which were performed to assure the wear scar detection via optical and confocal microscopy. Friction evolution was also analyzed during the tests. The materials considered for the pin were PTFE and TFM®, a molecularly modified virgin PTFE, which is characterized by a better load carrying capacity, lower gas permeability, and better mechanical properties than the virgin PTFE. For the counterpart (disc), both uncoated and H-DLC (Diamond Like Carbon) coated Al 6082-T4 alloy were considered.

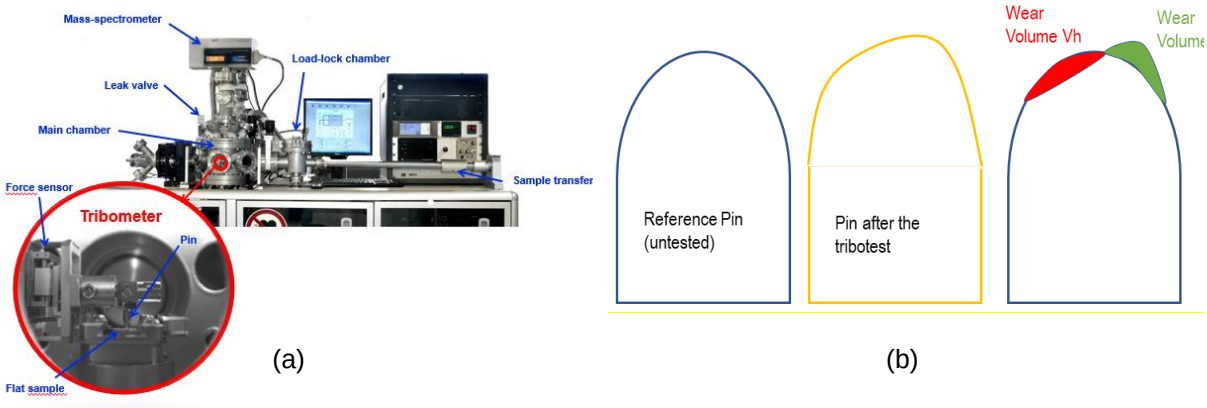

Figure 7. Tribological tests setup. a) Ultra Hight Vacuum tribometer used for tribological tests. b) Representation of the wear volume of the Pins determined via confocal microscopy.

The wear volume of the Pin after the tribological test has been calculated via confocal microscopy, obtaining the hole volume (Vh) and peak volume (Vp), according to the diagram presented in Fig. 7b. The analysis of the wear scars has been carried out via optical and scanning electron microscopy, including compositional analysis by energy dispersive x-ray spectroscopy. The selection of those materials as potential candidates for TEG has been done based on previous research studies where the use of PTFE

and a-C:H DLC as dielectric materials provided better tribological and triboelectric behavior than the materials considered as “gold standard” for this application (PTFE and Aluminium) [21][22].

According to previous research studies, high hydrogen content (H>30%) DLC coatings with moderate hardness (5—15 GPa) values might be the best candidates to reach superlubricity and low wear properties against PTFE under Mars environmental conditions [23]. Hence, different a-C:H DLC coatings have been deposited from the PECVD technique by varying C_2H_2 and bias voltage application to obtain high hydrogen content films. 5 Pa pressure and -300V bias voltage process parameters have been selected to achieve the best characteristics in terms of hydrogen contents and mechanical properties of all deposited coatings. Fig. 8a shows the cross-section SEM micrograph of the a-C:H DLC coating selected for tribological tests.

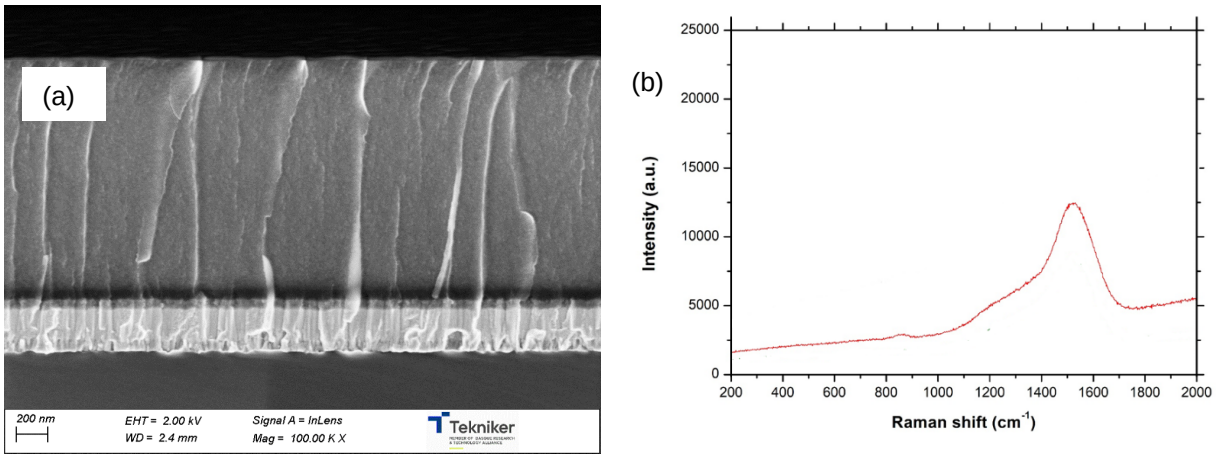

Figure 8. DLC developed for this work. a) Cross section SEM micrograph of a-C:H DLC film by PECVD i4. b) Raman spectra of DLC films developed.

Raman spectroscopy has been considered an indirect tool to measure hydrogen content on the a-C:H DLC film. A higher PL signal and G peak shift towards more negative values is indicative of higher hydrogen contents. If G position lies at 1530 cm^{-1} or lower, it can be concluded that the coating has hydrogen content higher than 35%. Fig. 8b shows the Raman spectra of the DLC produced for the tribological tests. As indicated in Tab. 2, the G position lies at 1523 cm-1(corresponding to H%>40%) and a hardness value measured via nanoindentation has been 11GPa.

Table 2. Summary of Raman and Nanoindentation results of the a-C:H DLC considered for tribological tests.

Sample	a-C:H DLC
G peak intensity (a.u.)	>10k
G position (cm^{-1})	1523
Hardness (GPa)	11
Estimated H(at%)	40+

Fig. 9 and 10 show the confocal microscopy characterization of PTFE pins before and after tribological tests, considering uncoated Aluminium and H-DLC coated Al as counterparts, respectively.

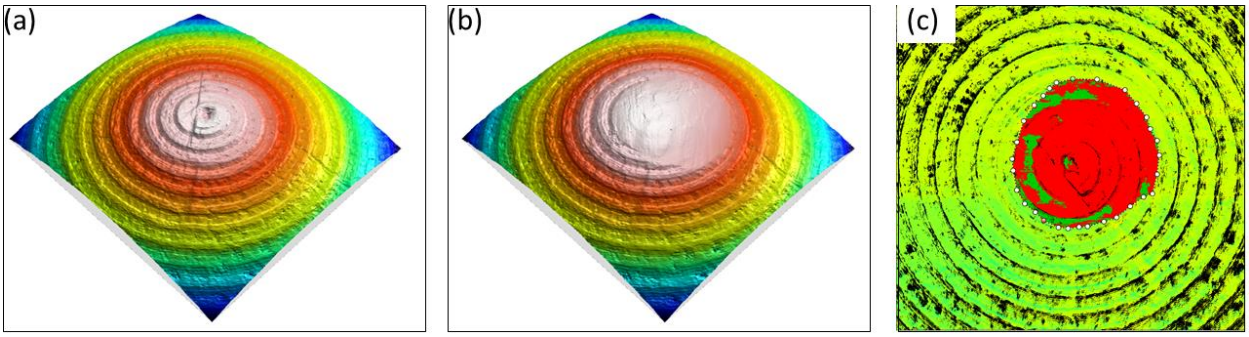

Figure 9: Confocal microscopy characterisaton of the contact surface of the PTFE pin before a) and after b) the tribological test, considering uncoated Aluminium as counterpart. c) wear volume (illustrated in red) of the pin.

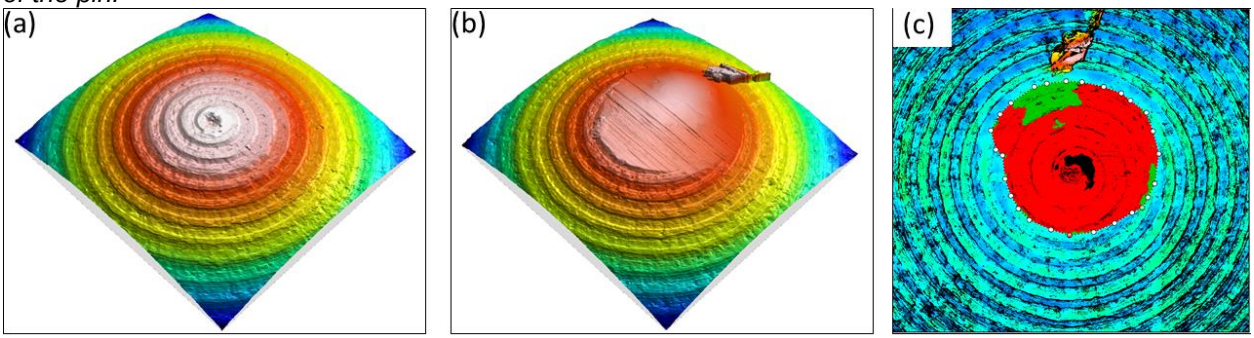

Figure 10. Confocal microscopy characterisaton of the contact surface of the PTFE pin before a) and after b) the tribological test, considering H-DLC coated Aluminium as counterpart. c) wear volume (illustrated in red) of the pin.

Optical microscopy inspection of the PTFE pins after tribological tests showed polymer degradation when uncoated Aluminium is considered as a counterpart (Fig. 11c). Thermal degradation of the polymer has been confirmed via EDX showing the lack of Aluminium debris adhesion to the contact surface of the pin. Polymer particle adhesion to the uncoated Al surface is also noticed in (Fig. 11a). This adhesion behavior of the PTFE was also observed when H-DLC coated Al is considered as a counterpart. However, no signs of PTFE degradation has been detected (Fig. 12). Hence, in terms of polymer integrity, the use of H-DLC coated Al as a counterpart guarantees better tribological performance.

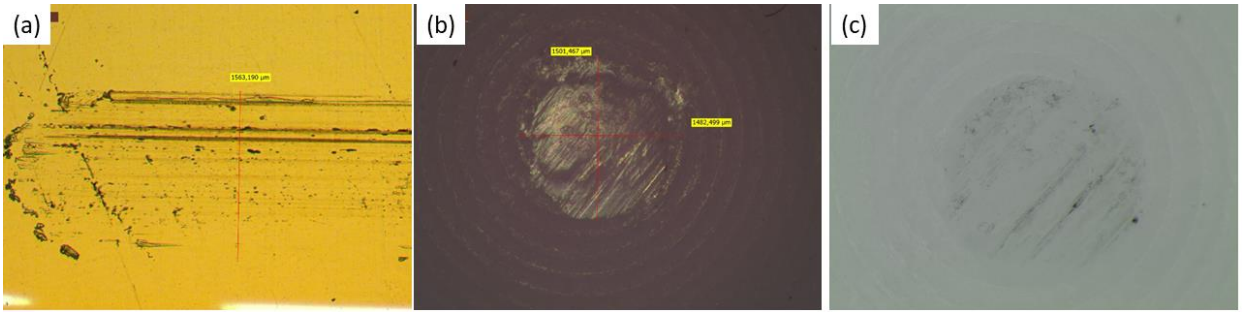

Figure 11. Optical microscopy characterisation of the uncoated Al sample (a) and the Pin of PTFE after the tribological test.

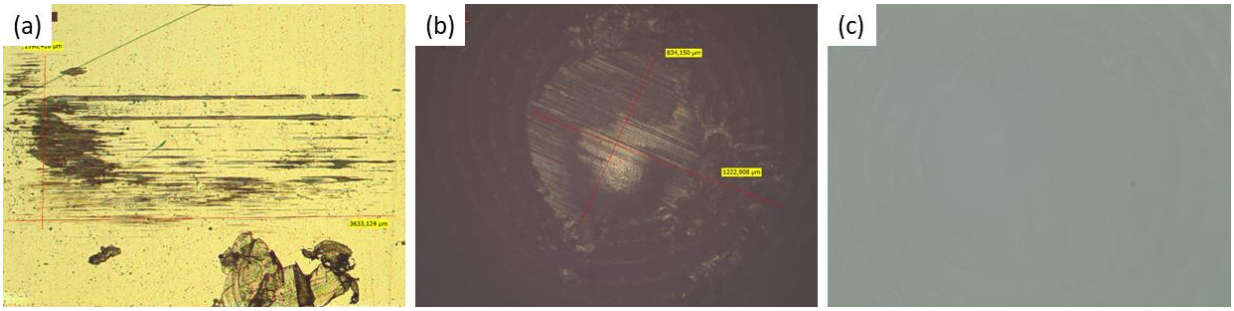

Figure 12. Optical microscopy characterisation of the H-DLC coated Al sample (a) and the Pin of PTFE after the tribological test.

Fig. 13 shows the polymeric Pin wear volume after tribological tests as a function of the tribopair selected. According to these results, the selection of TFM® as polymeric part of the TEG would provide better tribological behavior, characterized by a minimum wear behavior compared to PTFE. The time evolution of the coefficient of friction (COF) also confirms the better tribological performance corresponding to the TFM® + H-DLC coated Al tribopair.

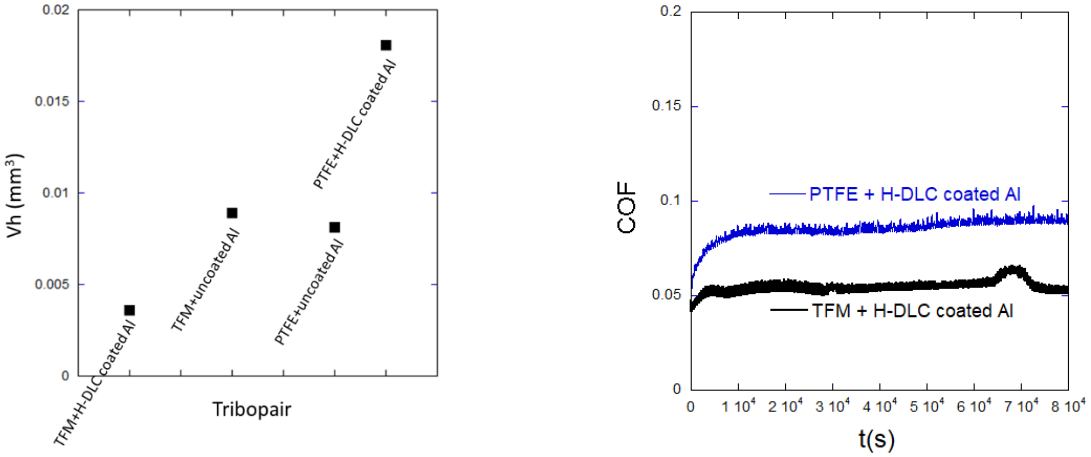

Figure 13. Tribological tests resutls. a) Wear volume after tribological tests (80000 s time duration) for different tribopairs,calculated via confocal microscopy. b) Time evolution of the Coefficient of Friction for selected tribopairs.

The following materials have been selected as the best candidates for experimentation. For polymeric materials: virgin PTFE, TFM® (a molecularly modified virgin PTFE). Then, the Aluminum Al6082 has been chosen as the metallic element for energy generation, and finally, Diamond-like carbon (DLC) coating has been used as a solid lubricant to improve the lifetime values given by the Aluminum and maintain the power generation. In this work, 3 DLCs have been developed and tested: a-C:H:W with H> 35 %, a-C:H:W + a-C:H, and a-C:H with H>40%.

Hydrogenated DLC and PTFE have been selected as dielectric pairs due to their highest power density, as well as their potential use as good solid lubricants/films. Abrasion resistance, lubrication ability, durability, and aging effects have been limitations of those materials - these problems have been solved by optimizing the coating architecture (adhesion layer optimization and multilayer architecture to realize residual stresses) and material microstructure (considering PTFE composites) based on lab-scaled tribology test results.

Triboelectrical tests

After the tribopair selection the trade-off generator has been designed and manufactured for the triboelectric test to study the performance under different Mars atmospheric conditions (see Fig. 14). To carry out the test, mechanical parts have been manufactured for triboelectric tests. The tribometer has been inserted in a vacuum chamber (called Titan) to carry out the tests.

Tests have been performed for various pressure values, in a sweep from 1000 mbar to 1 mbar with Earth atmospheric composition, vacuum level measurement until 0.2 mbar, and inverted sweep to the first point but in this case with simplified Mars atmospheric composition (CO_2 gas inserted in the chamber).

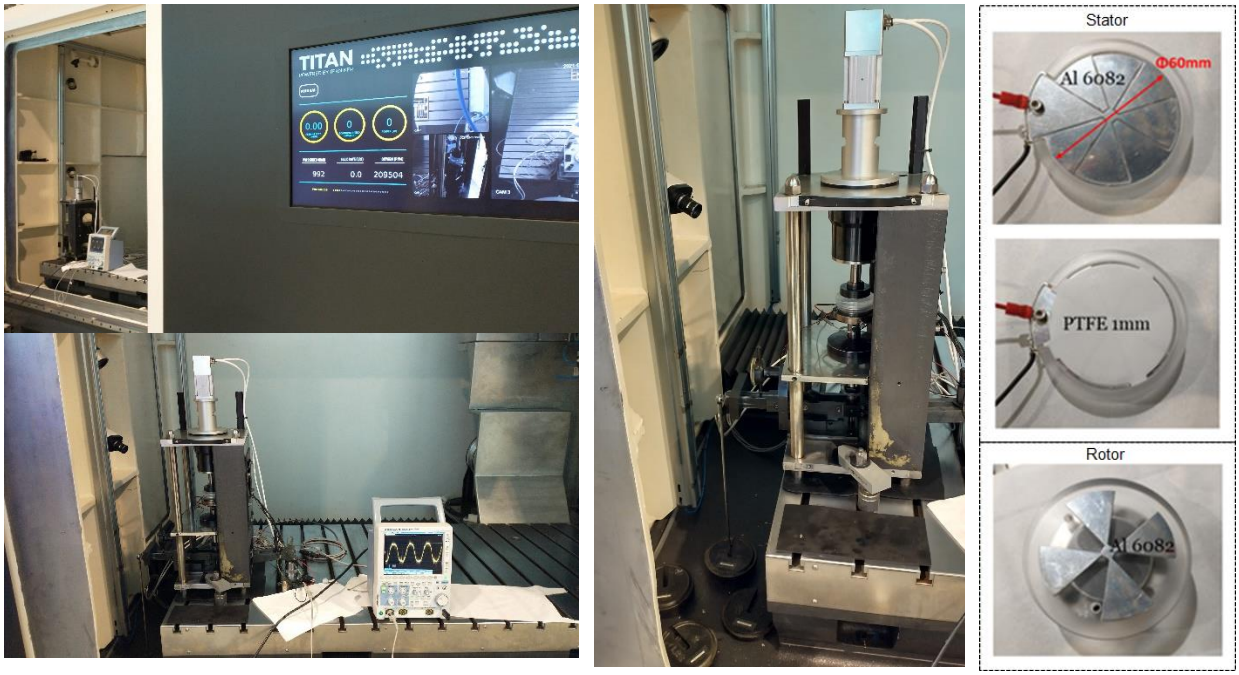

Figure 14. Test setup. Titan machine to reproduce Mars atmosphere, Falex rotatory tribometer, and manufactured trade-off breadboard to very the power generation of the TEG generator.

During the tests, the oxygen ppm have been continuously checked to verify if the atmospheric composition inside the Titan chamber is representative of Mars atmospheric composition conditions. For example, with Earth atmosphere, the O_2 ppm are around 210,000 and at the same pressure but with CO_2 the O_2 ppm are 9419, being CO_2 atmospheric composition 95.51%. After validation of test set-up, the triboelectrical tests to validate the better operation of TEG under Mars atmospheric composition and with Earth atmospheric pressure have been started.

Tests to analys voltage generation

After the first test, some initial conclusions on the TEG generator design have been achieved: TEG generator must be pressurized at least to 1000 mbar pressure with Mars atmospheric composition (95 % CO_2) to ensure a viable power generation. As it is shown in Fig. 15 and Tab. 3, the improvement at 1000 mbar pressure level is around 30-40 % in comparison with Earth atmospheric condition. The pressure and the CO_2 are the two main parameters that really affect the output voltage level which decreases at lower pressure levels (CO_2 effect is also decreased due to the Paschen law). In higher pressure levels the CO_2 effect on the materials increases the output voltage level (in comparison with air), corroborating the results of the tests with the literature.

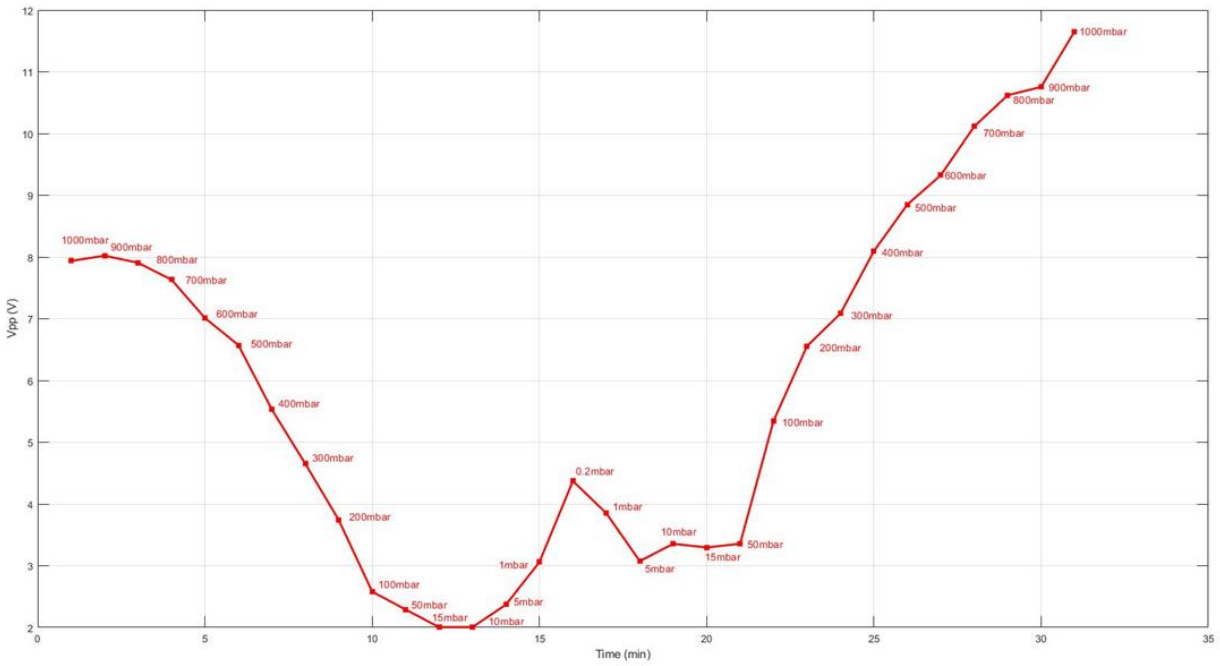

Figure 15. TEG generator voltage generation with pressure and atmospheric composition changes.

Table 3. Achieved output voltage values and comparison between Earth and Mars atmospheric changes.

Pressure (mbar)	Vpp Earth atm (V)	Vpp Mars Atm (V)	Increase (V)	Increase (%)
1000	7.94	11.65	3.71	31.85
900	8.02	10.76	2.74	25.46
800	7.91	10.62	2.71	25.52
700	7.63	10.12	2.49	24.60
600	7.01	9.33	2.32	24.87
500	6.57	8.85	2.28	25.76
400	5.53	8.10	2.57	31.73
300	4.65	7.09	2.44	34.41
200	3.74	6.56	2.82	42.99
100	2.58	5.35	2.77	51.78
50	2.29	3.35	1.06	31.64
15	2	3.30	1.3	39.39
10	2	3.35	1.35	40.30
5	2.37	3.07	0.7	22.80
1	3.06	3.85	0.79	20.52
0.2	4.37		-	-

The curve in Fig. 15 validates the work hypothesis and sets a roadmap for the generator design (the CO_2 effect is again clearly observed). In this sweep, the output voltage level at 1000 mbar is improved by 31.84%. Thus, to obtain the best working conditions, the generator must be pressurized at 1000 mbar with the Mars atmosphere composition.

In addition, the COF and Torque of the generator have been measured during two tests (Fig. 16). The main goal has been to study if Mars atmospheric composition in Earth atmospheric pressure (CO2 %95, 1000 mbar) has any significant effect on tribological parameters.

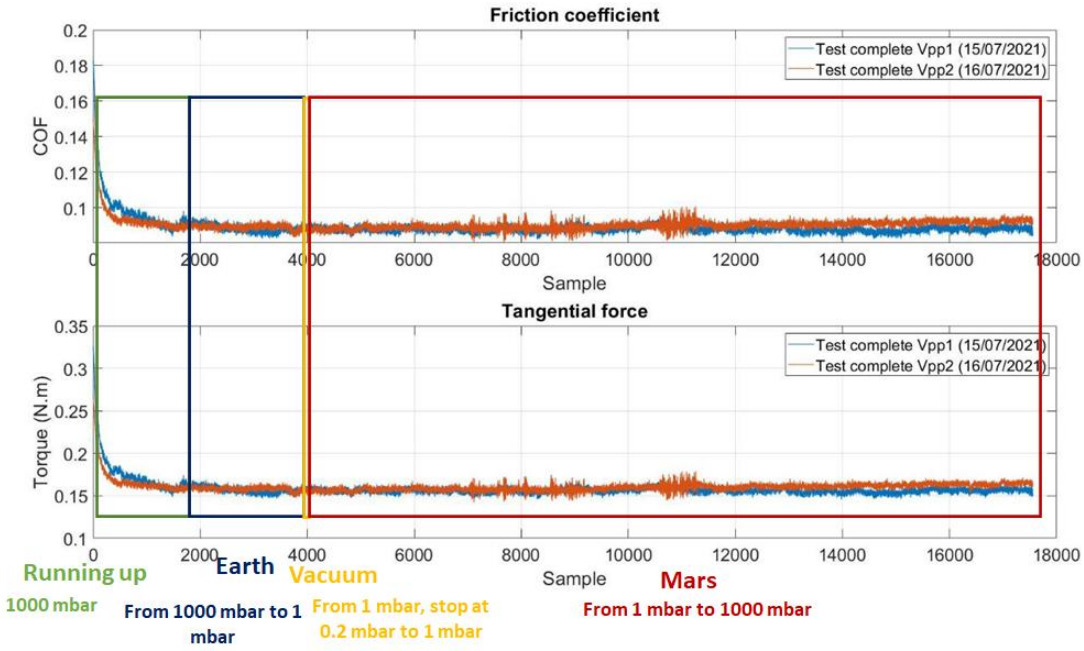

Figure 16. COF and Torque values during two complete sweep tests.

No variation has been observed in these two parameters with the change of pressure, so the conclusion is that the pressure variation doesn't make significant changes in the wear and in the COF of the TEG generator.

Conclusions

The viability of producing energy with a wind rotatory TEG generator under Mars atmospheric conditions has been demonstrated. The proposed turbine design works properly under Mars wind and atmospheric conditions, with the best tribopair PTFE/DLC (H>40%). The system should be able to work for at least 26 months due to the launch window between Earth and Mars and the tribopair selected should ensure this requirement. In addition, the generator must be pressurized up to 1000 mbar using with Mars atmospheric composition to achieve the higher efficiency in terms of power generation. Based on these results the wind turbine and the TEG generator are considered ready for the detailed design phase. The next steps are the manufacturing, assembly of the TEG with turbine which will be subjected to testing in a wind tunnel to validate the system under laboratory conditions.

References

[1]. Wang, P., Pan, L., Wang, J., Xu, M., Dai, G., Zou, H., Dong, K., & Wang, Z. L., An Ultra-Low-Friction Triboelectric-Electromagnetic Hybrid Nanogenerator for Rotation Energy Harvesting and Self-Powered Wind Speed Sensor. ACS Nano, 12(9), 9433–9440, 2018. https://doi.org/10.1021/acsnano.8b04654.

[2]. Z.L. Wang et al., Triboelectric Nanogenerators, Hybrid Electromagnetic and Triboelectric Nanogenerator, Chapter 12, Hybrid Cell Composed of Triboelectric Nanogenerator, Green Energy and Technology, Springer International Publishing Switzerland 2016, DOI 10.1007/978-3-319-40039-6_12.

[3]. James, G. H., & Chamitoff, Gregory, D. C. B. (1999). Design and Resource Requirements for successful wind energy production on mars. November 2014.

[4]. Hemmat, A., Nguyen, C., Singh, B., Wylie, K., Zimmerman, D., Kastor, R., & James, G. Conceptual Design of a Martian Power Generating System Utilizing Solar and Wind Energy. Second Annual HEDS-UP Forum, 131–146.

[5]. C. Holstein-Rathlou, P.E. Thomas, J. Merrison , J.J. Iversen, Wind turbine power production under current Martian atmopsheric conditions, Mars Workshop on Amazonian Climate 2018 (LPI Contrib. No. 2086).
[6]. Seol, M. L., Han, J. W., Moon, D. Il, & Meyyappan, M. (2017). Triboelectric nanogenerator for Mars environment. Nano Energy, 39(May), 238–244. https://doi.org/10.1016/j.nanoen.2017.07.004.
[7]. T. Matsuyama, H. Yamamoto, Charge relaxation process dominates contact charging of a particle in atmospheric conditions, J. Phys. D. Appl. Phys. 28 (1995) 2418–2423.
[8]. S.Brusca, "Design of a vertical-axis wind turbine: how the aspect ratio affects the trubine's performance," International Journal of Energy and Enviroment Egineering, 2014.
[9]. S. Zanforlin, "Effects of the Reynolds number and the tip losses on the optimal aspect ratio of straight-bladed Vertical Axis Wind Turbines," Energy, no. 148, pp. 179-195, 2018.
[10].X. Sun, "Aerodynamic performance and characteristic of vortex structures for Darrieus wind turbine I. Numerical method and aerodynamic performance.," Journal of Renewable and Sustainable Energy, 2014.
[11].Q. Li, "Effect of number of blades on aerodynamic forces on straight-bladed Vertical Axis Wind turbine," Energy, 2015.
[12].M. Shiono, "An experimental study of the characteristics of a Darrieus turbine for tidal power generation," Electrical Engineering in Japan, vol. 132, 2000.
[13].Blackwell, "Wind tunnel performance data for the Darrieus wind turbine with NACA0012 blades".
[14].G. Bedon, "Computational assesment of the DeepWind aerodynamic performance with different blade and airfoil configurations," Applied energy, 2015.
[15].Klimas, "Tailored airfoils for vertical axis wind turbines," 1984.
[16].Kadlec, "Characteristics of future vertical axis wind turbines," 1982.
[17].J. H. Strickland, "Darrieus turbine: a performance prediction model using multiple streamtubes".
[18].Klimas, "Effgects of blade preset pitch/offset on curved-blade Darrieus vertical axis wind turbine performance," 1981.
[19].T. Friedler, "Blade offset and pitch effects on a high solidity vertical axis wind turbine," Wind Engineering, vol. 33, 2009.
[20].S.H.Ramaswamy et al. “Investigation of diamond – like carbon films as a promising dielectric material for triboelectric nanogenerator” Nano Energy 60 (2019) 875-885.
[21].S.H.Ramaswamy et al. “Development of Highly Durable Sliding Triboelectric Nanogenerator Using Diamond – Like Carbon Films” Tribology Online V15, No.2 (2020) 89-97).
[22].Andersson, J., Erck, R. A., and Erdemir, A. Frictional behavior of diamondlike carbon films in vacuum and under varying water vapor pressure. Surf. Coat. Technol., 2003, 163–164, 535–540.